

# Scene Graph Generation from Hierarchical Relationship Reasoning

Bowen Jiang, Camillo J. Taylor

University of Pennsylvania

{bwjiang, cjtaylor}@seas.upenn.edu

## Abstract

*This paper describes a novel approach to deducing relationships between objects in a visual scene. It explicitly exploits an informative hierarchical structure that can be imposed to divide the object and relationship categories into disjoint super-categories. Specifically, our proposed scheme implements a Bayes prediction head to jointly predict the super-category or type of relationship between the two objects, along with the detailed relationship within that super-category. This design reduces the impact of class imbalance problems. We present experimental results on the Visual Genome and OpenImage V6 datasets showing that this factorized approach allows a relatively simple model to achieve competitive performance, especially on predicate classification and zero-shot tasks.*

## 1. Introduction

This work considers the Scene Graph Generation problem proposed by Johnson et al. in [11]. In this framing, the system’s goal is to deduce the objects in a given image and the relationships between them. Standard object detection [27, 29, 19, 1] or segmentation [8, 20, 30, 2] algorithms focus on identifying each object instance in an image separately. Scene graph generation algorithms, in contrast, represent the whole scene as a directed graph. They regard each object instance as a node in the graph and capture possible relationships between each pair of instances as an edge. Triplets of a subject, a relationship, and an object, like  $\langle \text{person}, \text{wear}, \text{skirt} \rangle$  and  $\langle \text{car}, \text{on}, \text{road} \rangle$ , form essential components of scene graphs, and such regularly appearing structures in images are also called *motifs* [41]. The rich knowledge encoded in scene graphs can be used for various downstream tasks, including image retrieval [23] and visual scene understanding [25, 11].

Zeller et al. [41] observe that the categories associated with the subject and object instances in an image are strongly predictive of the relationship between them. For example, the relationship between a “man” and a “shirt” is likely to be “wears”. The authors go further and show

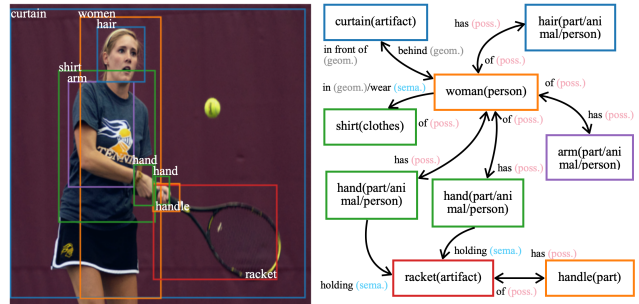


Figure 1. Example of a ground-truth scene graph. Each bounding box represents an object, labeled by its category and super-category. Arrows represent relationships between objects. The colors of the labels indicate the relationship super-categories: geometric, possessive, and semantic.

that when the objects in a dataset are divided into super-categories such as “Animal”, “Vehicle”, and “Furniture”, and the relationships between objects are similarly divided into super-categories such as “Geometric”, “Possessive”, and “Semantic”, the object categories and super-categories become strongly predictive of the relationship super-categories. For example, the relationship between a person and an article of clothing is likely to be possessive in nature. Based on this observation, the authors strongly argue for approaches that condition relationship predictions on the subject and object categories.

We build on this idea by proposing a new approach to scene graph construction, which directly exploits an informative hierarchical structure that can be imposed to divide the object and relationship categories into disjoint super-categories. We show that a relatively straightforward network that exploits this hierarchical structure can outperform state-of-the-art methods. Specifically, we propose a network that considers each subject-object pair in an image and produces several outputs, including a scalar value indicating whether two objects are connected by a relationship, the probability that the relationship, if it exists, belongs to each relationship super-category, and the conditional probability that the relationship has a specific class given the relationship super-category. The resulting network effectively

captures a structure from the Bayes’ rule where the probabilities associated with the super-categories serve to steer the attention of the network to the most profitable lines of interpretation. Numerical experiments demonstrate that our method *HierMotif* significantly improves performance, especially on the predicate classification tasks, by this form of hierarchical relationship reasoning.

The structure of this manuscript is as follows. Section 2 discusses some related work. Section 3 discusses details of our model, including the local Bayes predictor and an optional transformer encoder that can be used to refine the local results. Finally, Section 4 presents the experiments.

*To summarize our contributions:*

1. We show that a simple scene graph generation model can achieve superior performance by leveraging object and relationship hierarchies.
2. We propose a novel classification scheme inspired by Bayes’ rule that jointly predicts the relationship super-category probabilities and the conditional probabilities of the relationships within each super-category.
3. We propose a direction-aware multiplicative masking scheme for our classifier, and a dynamic batch sizing algorithm for efficient batch-wise training.

## 2. Related Work

Our work considers the scene graph generation problems proposed in [11] and [22]. Many authors have approached the problem from the graphical neural networks perspective [31, 37, 39, 18, 3, 12]. IMP [37] uses iterative message passing to update node and edge features in a bipartite graph. Graph-RCNN [39] prunes unlikely relationships and uses an attentional graph convolution network [13] to integrate global contexts and update nodes and edges.

Recurrent neural networks [41, 37, 4, 6] have also played important roles in scene graph generation as a means for integrating global context information across the image. For example, node and edge features in [37] are represented by two GRUs [4], which take incoming messages and produce new hidden states. Neural Motifs [41] investigates the repeated motif structures in scene graphs and captures global contexts with bidirectional LSTMs [10].

In their work on Neural Motifs, Zellers et al. [41] analyze scene graphs in the Visual Genome [15] dataset and divide the 150 most frequently encountered object categories into 17 super-categories and the 50 most frequently encountered relationship categories into 3 relationship super-categories: *geometric*, *possessive*, and *semantic*, as illustrated in Table 1. However, their proposed algorithm does not explicitly exploit the super-categories they identify. Our work follows their super-category classifications and fully utilizes this hierarchy information. We discover that the median relative frequency of a relationship label is only 0.17%,

but when we divide them into super-categories, this median frequency increases to 0.79% (geometric), 1.4% (possessive), and 2.3% (semantic), respectively.

Super-categories	Categories	Num
Geometric	above, behind, between, near, ...	15
Possessive	belonging to, has, of, part of, ...	11
Semantic	wears, carrying, eating, riding, ...	24

Table 1. The relationship hierarchy in [41] and some examples under each super-category. Our work follows the same definitions.

In recent years, BGT-Net [6] utilizes a bidirectional GRU for instance-level communications, an object transformer encoder to predict instance categories, and another edge transformer encoder to generate edge information for every instance. HC-Net [28] works on scene graph generation with hierarchical contexts, rather than the hierarchies of objects and relationships we exploit. GPS-Net [18] focuses on recovering the direction of the relationship edges and understanding the relative priority of the nodes in the graph within a novel message-passing scheme. RTN [14] presents a relation transformer network with a node-to-node encoder and a node-to-edge decoder. RelTR [5] also employs a Detection Transformer (DETR) [1] backbone, but it proposes a complicated triplet decoder network with three sub-modules and takes subject and object queries as input tokens. [38] establishes a unified conditional random field to model the distribution of objects and relationships jointly. Besides, [33] offers an energy-based framework instead of cross-entropy loss to incorporate the structure of the scene graph.

## 3. Method

### 3.1. Notation

A scene graph  $G = \{V, E\}$  is a graphical representation of a given image  $I$ . The set of vertices  $V$  consists of  $n$  object instances, including their bounding boxes  $\{b_i \mid b_i \in \mathbb{R}^4\}$ , the object categories  $\{c_i \mid c_i \in \mathbb{N}\}$ , and the object super-categories  $\{sc_i \mid sc_i \in \mathbb{N}\}$  for each  $c_i$ . We sometimes use the word “instances” to cover “subjects” and “objects”. The set of edges,  $E$ , consists of relationships  $\{r_{ij} \mid r_{ij} \in \mathbb{N}\}$  between each pair of instances, and the associated relationship super-category  $\{sr_i \mid sr_i \in \mathbb{N}\}$ . Both  $i$  and  $j$  ranges from 1 to  $n$ , so the total number of possible  $r_{ij}$  is  $n^2$ . For every possible edge we predict a connectivity score  $\{e_{ij} \mid e_{ij} \in [0, 1]\}$  which models whether a particular subject and object are connected.

### 3.2. Scene Graph Construction

Our basic scene understanding system in Figure 2 constructs a scene graph by considering each pair of object instances in turn and predicting whether or not they are related and, if so, what kind of relationship pertains. We refer to

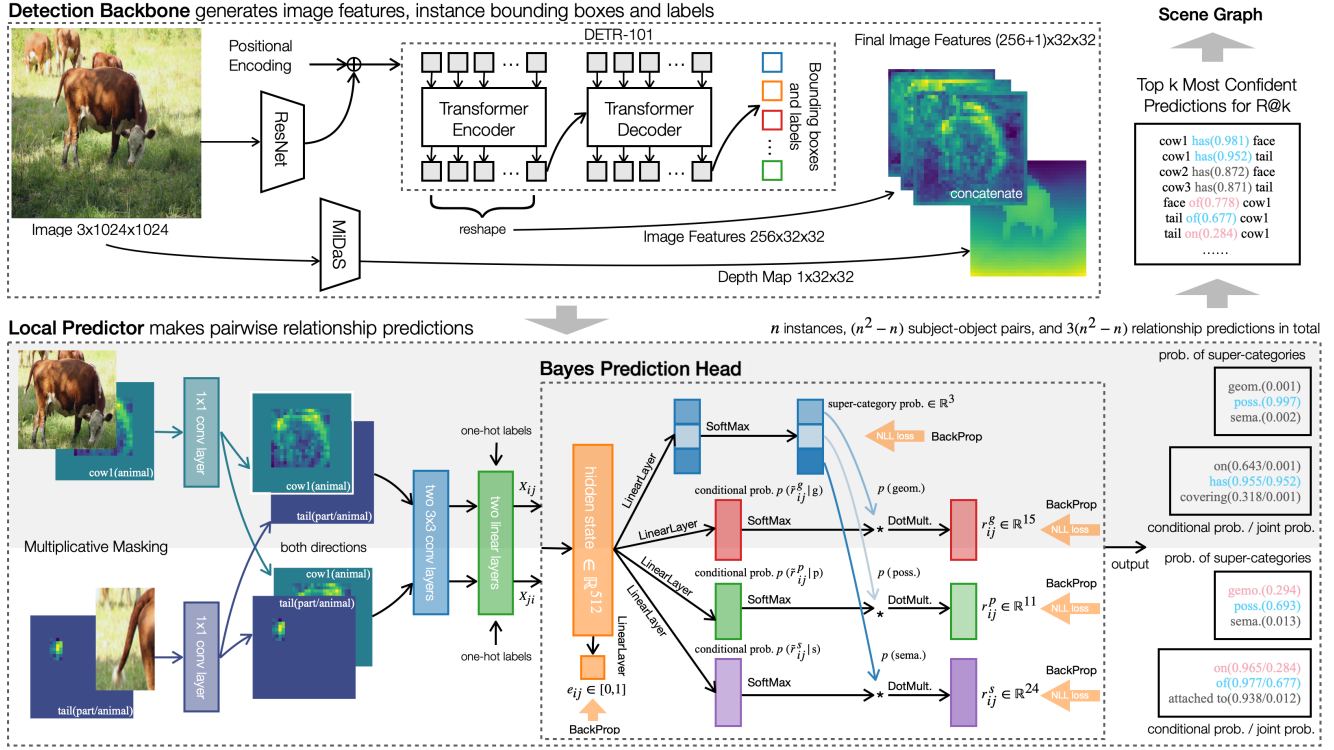


Figure 2. Illustration of our scene graph construction scheme. The DETR detection backbone generates image features, instance bounding boxes and labels. The local predictor simply predicts pairwise relationships. Given two object proposals  $i$  and  $j$ , we do two separate passes through our relationship network, one with  $i$  as the subject and  $j$  as the object, and the other with  $j$  as the subject and  $i$  as the object. Their feature maps are concatenated as  $X_{ij}$  and  $X_{ji}$  as two possibilities evaluated individually by the Bayes prediction head. The head predicts the super-category distribution and the conditional probabilities under each super-category. It produces three hypotheses for the relationship, one for each super-category. Each of these hypotheses is scored by computing the product of the edge connectivity score and the maximum entry in each of the three final vectors. In the results, pink predicates are true positive, blue predicates are reasonably true predictions but not annotated in the dataset, and gray predicates are false positive.

this as a local prediction system to distinguish it from other approaches that consider more global scene information.

**Object detection backbone** We follow the most common two-stage model design [37, 39, 41, 18, 6] to first predict object bounding boxes and labels by a pre-trained object detection backbone, and then predict relationships between objects. We adopt the DETR [1] object detection module as the front end for our scene graph generation system. DETR has a ResNet-101 feature extraction backbone [9, 32], followed by a transformer encoder [1, 36]. Next, a transformer decoder and a feed-forward head [1, 36] predict the final set of object predictions in parallel. Once DETR outputs instance categories, we associate them with their super-categories. Finally, MiDaS [26] single-image depth estimation network is applied to the input image.

**Direction-aware multiplicative masking** After we have extracted the image features, we consider each pair of object instances as shown in Figure 2. Considering every per-

mutation of instance pairs allows the system to cover all options. For every subject-object pair, we construct a combined feature tensor by converting the bounding boxes associated with the subject and object into binary masks, and then multiplying them elementwise with the image features to produce two feature tensors, one for the subject and one for the object, which is concatenated and passed on to the next stage. Note that the order of the two feature tensors is crucially important since motifs such as *<bike, has, wheel>* and *<wheel, of, bike>* hinge on which instance is considered the subject and which the object. Given two object proposals  $i$  and  $j$ , we do two separate passes through our relationship network, one with  $i$  as the subject and  $j$  as the object, and the other with  $j$  as the subject and  $i$  as the object. We avoid using a simple union mask of each subject-object pair, since the two bounding boxes may have significant overlap and the edge direction information would be lost. Some works crop instances by their regions of interest and resize them to a uniform size to form the object feature vectors [41, 6, 40]. Our direction-aware multiplica-

tive masking strategy maintains the instance size information, the spatial locations of each instance in the image, and the relative locations between each subject-object pair. Our ablation studies show that this approach significantly improves performance.

The subject-object feature tensors are passed to a network with 2 convolutional layers and 2 linear layers which produces a 512-dimensional hidden state vector  $X_{ij}$  as shown in Figure 2. This hidden state vector is passed to the Bayes prediction head along with 4 one-hot vectors that encode the categories and super-categories associated with the subject and object.

**Bayes prediction head** The Bayes prediction head is structured to produce several interpretable quantities, inspired by the Bayes' rule. The first output  $e_{ij} \in [0, 1]$  is a scalar connectivity score, indicating the likelihood that object instances  $i$  and  $j$  are related. The network also produces three scalar values  $[p(g), p(p), p(s)]$ , representing the probabilities that the relationship, if it exists, belongs to the geometric, possessive or semantic super-categories respectively. Finally, the network produces three vectors that are interpreted as conditional probability distributions:  $p(\tilde{r}_{ij}^g \mid g) \in \mathbb{R}^{15}$  denotes the probability that the relationship should be labeled as each of the 15 categories under the geometric relationship super-category, conditioned on the relationship belonging to that super-category. Similarly,  $p(\tilde{r}_{ij}^p \mid p) \in \mathbb{R}^{11}$  and  $p(\tilde{r}_{ij}^s \mid s) \in \mathbb{R}^{24}$  denote the conditional probabilities associated with the possessive and semantic super-categories respectively.

Figure 2 and Equations 1-5 show how these quantities are combined to produce final classification results trainable via back-propagation. The output score vectors associated with each relationship category,  $r_{ij}^g \in \mathbb{R}^{15}$ ,  $r_{ij}^p \in \mathbb{R}^{11}$ , and  $r_{ij}^s \in \mathbb{R}^{24}$ , are simply the conditional probability vectors multiplied by the associated super-class probabilities.

$$e_{ij} = \text{Sigmoid} \{ X_{ij}^\top W^{\text{conn}} \} \quad (1)$$

$$[p(g), p(p), p(s)] = \text{Softmax} \{ X_{ij}^\top W^{\text{sc}} \} \quad (2)$$

$$r_{ij}^g := p(\tilde{r}_{ij}^g \mid g) * p(g) = \text{Softmax} \{ X_{ij}^\top W^g \} * p(g) \quad (3)$$

$$r_{ij}^p := p(\tilde{r}_{ij}^p \mid p) * p(p) = \text{Softmax} \{ X_{ij}^\top W^p \} * p(p) \quad (4)$$

$$r_{ij}^s := p(\tilde{r}_{ij}^s \mid s) * p(s) = \text{Softmax} \{ X_{ij}^\top W^s \} * p(s) \quad (5)$$

The  $W$ s in these equations are the learnable linear layer parameter tensors.

The local prediction network finally outputs three relationship predictions, one for each super-category, by simply considering the maximum entry in each of the vectors  $r_{ij}^g$ ,  $r_{ij}^p$  and  $r_{ij}^s$ . The associated maximum entries are multiplied by the connectivity score,  $e_{ij}$ , to produce a final score for each relationship hypothesis. These scores are used to rank order the relationship hypotheses from all subject-object

pairs, and this ordering is used to suggest the most likely relationships in the scene. Note that in this structure, the super-category probabilities act to focus the network's attention on the appropriate conditional output heads.

Equation 1-5 can be summarized as follows:

$$[r_{ij}^g, r_{ij}^p, r_{ij}^s, e_{ij}] = \text{BayesHead} \{ X_{ij} \}. \quad (6)$$

**Dynamic batch sizing** One challenge in training our local prediction module efficiently stems from the fact that the images in the dataset typically contain different numbers of object instances and, therefore, contribute different numbers of ground-truth relationships to the training process. This can be a problem when we want to parallelize the training process with batch-wise operations.

To handle this problem, we propose a dynamic batch sizing scheme that can be effectively parallelized across multiple images in a training batch. The dynamic batching process is described in Algorithm 1, where `max_index` denotes the maximum number of objects detected in any image in the current batch.

---

#### Algorithm 1 Dynamic Batch Sizing

---

```

for k=2 thru max_index do
    empty mini-batch
    for all images in the batch with k or more objects do
        for j=1 thru (k-1) do
            Add the relationships between objects j and k
            to the mini-batch
        end for
    end for
    Update network parameters based on the
    relationships in the mini-batch
end for

```

---

### 3.3. Global context via motif-level attention

The local prediction scheme described in the previous sections constructs a scene graph by considering each pair of objects in the scene in turn and in isolation. We propose an optional third stage with a transformer encoder [36, 7] to extract global context information, which can be used to refine the local prediction outputs.

Since most scene graphs are sparse, we select a small subset  $S$  of hidden states  $\{X_{ij} \mid X_{ij} \in S\}$  associated with the most highly scored relationship predictions, so that the model can focus its computational effort on the most informative relationship predictions.

Values  $V$ , keys  $K$ , queries  $Q$  [36] for all  $X_{ij}$  in  $S$  and the associated self-attention weights can be calculated from:

$$V = X, K = X^\top W^K, Q = X^\top W^Q, \quad (7)$$

$$\text{Attention}(Q, K, V) = \text{SoftMax} \left( \frac{QK^\top}{\sqrt{d}} \right) V, \quad (8)$$

where  $X$  is matrix constructed by concatenating all the  $\{X_{ij} \mid X_{ij} \in S\}$ .  $W^V$  and  $W^K$  are two learnable matrices, and the scale factor  $d$  is used to stabilize the gradients [36]. The dot-product  $QK^\top$  between each pair of key and query produces the attention scores, representing how much attention each motif should pay to any other motifs. We also follow [36]’s suggestion on multi-head attention and add-and-norm layers. The resulting block is repeated several times to form the entire transformer encoder network.

The transformer encoder outputs a set of new embedding vectors  $\{Y_{ij} \mid X_{ij} \in S\}$ . And these vectors are added to the corresponding  $X_{ij}$  as a residual connection to refine the relationship predictions. More specifically, for every relationship in  $S$ , the refined relationship is computed from:

$$[\hat{r}_{ij}^g, \hat{r}_{ij}^p, \hat{r}_{ij}^s, e_{ij}] = \text{BayesHead} \{X_{ij} + Y_{ij}\}. \quad (9)$$

## 4. Experimental Results

### 4.1. Dataset

**Visual Genome** We perform comprehensive experiments on the Visual Genome dataset [15], following the same pre-processing procedure used in [37] to clean up object annotations. We consider the most frequent 150 object categories and 50 relationship predicates in the dataset. These are divided into 17 object super-categories and 3 relationship super-categories as defined in [41]. The dataset contains around 75.7k training images and 32.4k testing images. On average, each image in the dataset contains 11.5 object instances and 6.2 relationships.

**OpenImage V6** We follow the same data pre-processing provided by [17] to obtain a subset of the OpenImage V6 dataset [16] with relationship annotations. It has 601 object categories, 30 relationship categories, about 53.9k training images, and around 3.2k testing images.

### 4.2. Evaluation metrics

**Visual Genome** We employ the Recall@ $k$  (R@ $k$ ) [22] and mean Recall@ $k$  (mR@ $k$ ) [35] evaluation metrics that are widely used for this dataset. R@ $k$  measures the fraction of the ground-truth predicates that appear in the top  $k$  most confident predictions per image, the mR@ $k$  metric averages the recall score over all 50 relationship categories and, thus, provides an idea of how well the method performs across all of the relationship categories. A ground truth predicate matches a hypothesized relationship if the predicted relationship is correct, the subject and object labels match, and the bounding boxes associated with the subject and object both have  $\text{IOU} \geq 0.5$  with the ground-truth boxes.

In our hierarchical relationship scheme, each edge has three predictions per direction under three disjoint super-categories. Therefore, each directed edge outputs three individual candidates to be ranked in the top  $k$  most confident

predictions instead of one, as shown in Figure 2. Note that allowing three candidates per edge does not make the ranking problem easier, because the total number of candidates will be three times larger, and it is still challenging to put correct predicates in the top  $k$  ranking.

We also provide two more evaluation metrics, R@ $k^*$  and mR@ $k^*$ , which offer more insight into the accuracy of the prediction heads associated with each relationship super-category. For these metrics, if any of the three super-category output heads,  $r_{ij}^g$ ,  $r_{ij}^p$  or  $r_{ij}^s$ , correctly predicts the relationship, we score it as a match. We contrast this with the NG-R@ $k$  described in [24, 41], where “NG” represents “no graph constraint”. This score significantly surpasses R@ $k$ , but it loosely defines a “match” as long as any of the 50 predicates with non-zero scores match with the target without further restrictions. In contrast, our R@ $k^*$  is still quite strict, since predicates within the same super-category remain exclusive. In other words, each relationship hypothesis would have at most three chances to be marked correct.

Zero-shot recall (zsR@ $k$ ) [34] estimates the model’s ability to generalize its performance to unseen data. It calculates the R@ $k$  score for those  $\langle \text{subject}, \text{relationship}, \text{object} \rangle$  triplets that only appear in test data, but not in the training dataset.

**OpenImage V6** On this challenge we consider the standard evaluation metrics: Recall@50 (R@50), weighted mean average precision of relationships (wmAP<sub>rel</sub>), weighted mean average precision of phrases (wmAP<sub>phr</sub>), and the final score =  $0.2 \times R@50 + 0.4 \times \text{wmAP}_{\text{rel}} + 0.4 \times \text{wmAP}_{\text{phr}}$ . The weighted AP addresses the predicate class imbalance [42]. wmAP<sub>rel</sub> counts a match if both the subject and the object bounding boxes have  $\text{IOU} \geq 0.5$  with their ground-truths, and the  $\langle \text{subject}, \text{relationship}, \text{object} \rangle$  labels match with the target. Same for wmAP<sub>phr</sub> except it considers the union bounding box of the subject and object.

### 4.3. Evaluation modes

**Predicate classification** Predicate classification (Pred-CLS) separates the relationship prediction task from other procedures. Given a ground-truth set of object instances labels and bounding boxes, the model predicts relationships.

**Scene graph classification** In this task the model predicts subject, object, and relationship categories, given ground-truth subject and object bounding boxes. In our experiment, the DETR detection backbone outputs object bounding boxes and labels simultaneously without a separate region proposal network [29], so we match each ground-truth bounding box with the predicted bounding box with the largest IOU and use the predicted object label.

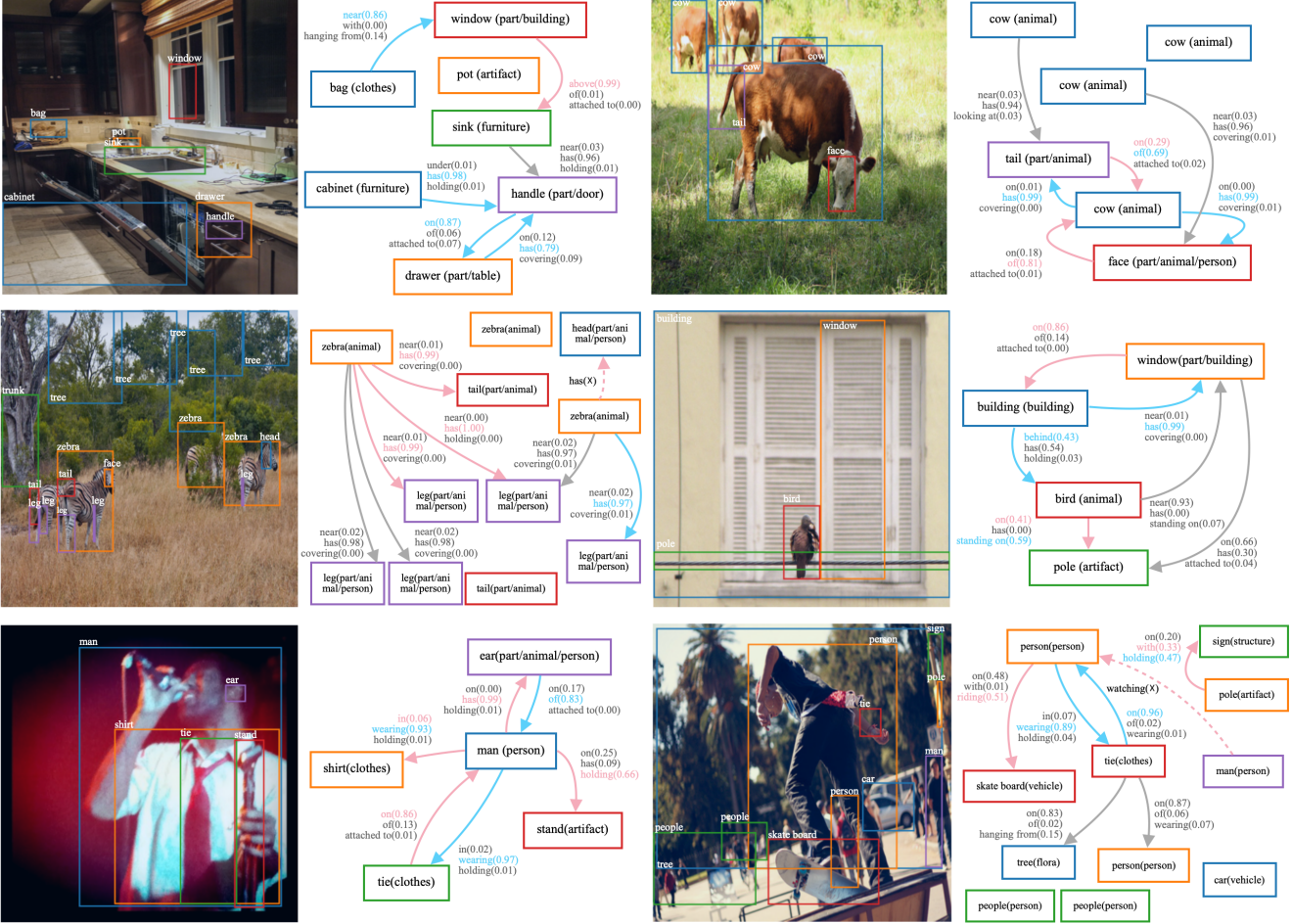


Figure 3. Illustrations of scene graphs produced by our model for the PredCLS task. All samples come from the Visual Genome test dataset. Each edge is annotated with 3 possible labels, one for each relationship super-category. The numbers show the system’s belief that that super-category estimate is the correct one. We show all edges that contain predicates among the top 5 most confident predictions and other true positive predictions among the top 20. We sketch four types of arrows: (1) solid pink arrow: contains true positive predicates. (2) dotted pink arrow: false negative predicates, relationships that are in the ground truth annotation that are missed. (3) solid blue arrow: represent reasonable true positives that are not annotated in the dataset. (4) solid gray arrow: represent false positive predicates. Recall can be calculated as num solid pink arrows / (num solid + dotted pink arrows).

**Scene graph detection** Scene graph detection (SGDET) requires the model to predict instance bounding boxes, object labels, and relationships. SGDET requires additional adaptations to the detection backbone because the predicted bounding boxes and labels are noisy and can degrade the model’s performance. For example, we add per-class NMS post-processing to avoid many unnecessary relationship predictions and dramatically reduce computation time. We also dismiss all subject-object pairs whose bounding boxes have no overlap [41]. Predicted instance categories are often inaccurate. The prediction will be regarded as wrong if the subject or object category is wrong, regardless of the relationships. To combat this, we duplicate the predicted bounding boxes twice in each image and consider the top two most confident object categories to improve the

likelihood of detecting the correct relationships. Furthermore, we account for the fact that some object categories are ambiguous. For example, if the dataset annotates an instance as “apple”, but the detector predicts it as “fruit”, the result should still be accepted.

#### 4.4. Training details

All models are trained on 4 NVIDIA V100 GPUs. The time to run inference on a typical image is around 1.5s. We leverage the pretrained DETR backbone provided by [17] under object detection tasks. The relationship prediction network is trained with a batch size of 32 for 3 epochs on Visual Genome, or 1 epoch on OpenImage V6, by the SGD optimizer with a learning rate of 0.002 and a step scheduler. We freeze the parameters of the DETR object detec-

Methods	PredCLS			SGCLS			SGDET		
	R@20	R@50	R@100	R@20	R@50	R@100	R@20	R@50	R@100
IMP [37]	-	44.8	53.1	-	21.7	24.4	-	3.4	4.2
GraphRCNN [39]	-	54.2	59.1	-	29.6	31.6	-	11.4	13.7
NeuralMotifs [41]	58.5	65.2	67.1	32.9	35.8	36.5	21.4	27.2	30.3
Motif+EB [33]	58.4	65.2	67.3	35.7	39.1	40.0	<b>24.3</b>	<b>31.7</b>	<b>36.3</b>
HC-Net [28]	59.6	66.4	68.8	34.2	36.6	37.3	22.6	28.0	31.2
GPS-Net [18]	60.7	66.9	68.8	<b>36.1</b>	<b>39.2</b>	<b>40.1</b>	22.6	28.4	31.7
BGT-Net [6]	60.9	67.3	68.9	<b>38.0</b>	<b>40.9</b>	<b>43.2</b>	23.1	28.6	<b>32.2</b>
RelTR [5]	<b>63.1</b>	64.2	-	29.0	36.6	-	20.2	25.2	-
HierMotifs* (ours)	<b>66.9</b>	<b>77.5</b>	<b>80.3</b>	34.6	38.8	<b>40.1</b>	<b>24.8</b>	<b>30.2</b>	31.8
HierMotifs (ours)	60.5	<b>73.2</b>	<b>77.9</b>	31.2	37.0	39.2	21.8	28.0	30.7
	mR@20	mR@50	mR@100	mR@20	mR@50	mR@100	mR@20	mR@50	mR@100
NeuralMotifs [41]	11.7	14.8	16.1	6.7	8.3	8.8	4.9	6.8	7.9
Motif+EBM [33]	14.2	18.0	19.5	8.2	10.2	11.0	5.7	7.7	9.3
GPS-Net [18]	17.4	21.3	22.8	10.0	11.8	12.6	6.9	8.7	<b>9.8</b>
BGT-Net [6]	16.8	20.6	23.0	<b>10.4</b>	<b>12.8</b>	<b>13.6</b>	5.7	7.8	9.3
RelTR [5]	<b>20.0</b>	21.2	-	7.7	11.4	-	6.8	<b>10.8</b>	-
HierMotifs* (ours)	<b>20.5</b>	<b>25.8</b>	<b>27.1</b>	<b>11.5</b>	<b>13.6</b>	<b>14.5</b>	<b>7.1</b>	<b>9.4</b>	<b>10.1</b>
HierMotifs (ours)	14.8	<b>21.5</b>	<b>24.9</b>	8.0	11.5	13.4	4.6	7.4	9.7

Table 2. Testing results for different methods on the Visual Genome dataset. Top two results are shown in **bold**, and “-” denotes results that are not reported. We use the evaluation metrics R@ $k$  and mR@ $k$ , except \* means R@ $k^*$  and mR@ $k^*$ . The last row of each sub-table shows that our method, HierMotif, outperforms most state-of-the-art methods on the PredCLS task by a large margin and has similar performance on SGCLS and SGDET. Each penultimate row shows that our three super-category prediction heads are even more effective at identifying the correct relationship.

tor while training the local predictor module. The optional transformer encoder is trained with the same batch size for 3 more epochs by the AdamW [21] optimizer with a learning rate of 0.005 and warmup steps [36], having other module parameters being frozen.

## 4.5. Results

**Visual Genome** Table 2 compares our results on Visual Genome to other state-of-the-art methods. Our model, HierMotif, significantly outperforms previous methods on R@50 and R@100 for the PredCLS task by 6 and 9 percent, respectively. The penultimate row of each sub-table reports our R@ $k^*$  and mR@ $k^*$  that highlight the strong performance of the super-category prediction subsystems. These results show that the individual Bayes prediction heads have successfully learned how to predict the relationships within each super-category. The strong mR@ $k$  scores indicate improved performance across all relationship categories. Furthermore, it suggests that the scheme allows the specialized prediction heads to concentrate more effectively on discriminating within their relationship super-categories.

Figure 3 shows some generated scene graphs for the PredCLS task on Visual Genome. The model generates a diverse set of predicates with high confidence to describe the visual scenes. We note that existing evaluation metrics may severely underestimate the model’s actual capabilities due to insufficient ground-truth annotations in the dataset. The model produces many reasonable predictions that align with human intuition but are not annotated in the dataset. They are marked with blue arrows in the figure. We believe

Methods	zsR@20/50		zs-mR@20/50	
	zsR@20	zsR@50	zs-mR@20	zs-mR@50
NeuralMotifs [41]	1.4	3.6	-	-
Motif+EB [33]	2.1	4.9	-	-
VC-TDE+EB [33]	9.6	15.1	-	-
Ours	<b>11.1</b>	<b>17.4</b>	<b>3.2</b>	<b>6.5</b>
Ours no rel-hier	9.9	15.5	2.8	4.2

Table 3. Zero-shot recall for the PredCLS task on Visual Genome dataset. In the last row, “no rel-hier” means no relationship hierarchy, i.e., the model without the Bayes prediction head.

generating a rich set of reasonable predicates is helpful in practical scene understanding.

The model sometimes gets confused on repeated instances of the same type. For example, it sometimes connects one cow to another nearby cow’s tail. We have also noticed cases in the dataset where the relationship between a subject and an object may be ambiguous; for example, a particular relationship may be annotated as *<tail, of, cow>* or *<tail, on, cow>*. Typically the two contending relationships belong to different super-categories, which our model handles quite naturally by reporting that two super-categories have likely predictions for an edge.

Table 3 shows the strong zero-shot performance of our model on Visual Genome. The bottom row shows an ablation study where we do not use the Bayes prediction head and observe an inferior performance.

**OpenImage V6** Table 4 demonstrates the experimental results on the OpenImage V6 dataset. It has an outstanding recall score, similar to the results on Visual Genome.

Our model makes predictions on all subject-object pairs and outputs the top 20 most confident predictions for each image, so its precision  $\text{wmAP}_{\text{rel}}$  still has space to improve, but  $\text{wmAP}_{\text{phr}}$  and the final score are already competitive.

Methods	R@50	wmAP <sub>rel</sub>	wmAP <sub>phr</sub>	score
SGTR [1]	59.9	37.0	38.7	42.3
RelDN [42]	74.9	35.5	38.5	44.6
GPS-Net [18]	77.27	38.78	40.15	47.03
BGT-Net [6]	78.0	<b>39.6</b>	40.8	47.7
Ours	<b>85.4</b>	33.1	<b>44.9</b>	<b>48.3</b>

Table 4. Testing results on the OpenImage V6 dataset. Top one results are shown in **bold**. The final score is prominent.

**Ablation studies** We provide ablation studies on Visual Genome in Table 5 to validate our key design decisions. Firstly, we investigate how our system would fare if we simply used a flat relationship categorization, instead of the hierarchical organization into three relationship super-categories with the Bayes prediction head. The performance is shown on the second row of the table, and it is much worse than the hierarchical baseline. Suggests that our hierarchical organization is improving performance, allowing our on-purposely simple relationship prediction scheme to perform competitively to other methods.

The third row shows the results if we ignore the super-categories associated with the object instances. It shows that object super-categories are useful, but not as critical as the relationship super-categories. Nevertheless, the decreases in mR@ $k$  suggest that the object super-category information helps share information across related classes and thus improves the performance, especially when the object categories are less frequently seen. The fourth row indicates that the image depth maps also help with the predictions.

In the fifth row, we examine the performance of a variant that does not use the direction-aware multiplicative masking scheme to extract subject and object features, but instead uses union bounding boxes. This variant does not perform as well as our baseline, indicating that the direction-aware scheme is beneficial.

The fifth and sixth rows investigate the value of adding the optional transformer structure with two slightly different parameter settings to refine the relationship predictions. These results indicate that this additional structure improves mR@ $k$  and mR@ $k^*$  but sacrifices a small amount of performance on the R@ $k$  and R@ $k^*$ . We conclude that our standard local prediction system is already strong and hypothesize that the DETR object detection backbone may already provide some global context via its transformer network.

The final several rows of the table show results obtained by varying various hyperparameters related to the SGDET task, specifically by changing the number of times we duplicate each predicted bounding box, as explained in Sec-

tion 4.3. We also show the result of varying the amount of non-maximal suppression applied to the bounding boxes produced by the DETR system during object detection.

In PredCLS	R@20	R@50	mR@20	mR@50
Final	<b>60.5</b>	<b>73.2</b>	14.8	21.5
No rel-hierarchy	53.2	63.3	10.8	13.6
No ins-hierarchy	59.4	71.8	13.7	19.6
No depth map	59.9	72.2	13.1	19.1
Union bbox	53.2	67.8	12.2	18.6
Add tf-enc s0.2	60.1	72.7	<b>16.7</b>	22.8
Add tf-enc s0.5	59.7	72.0	15.5	<b>23.4</b>

In SGDET	R@20	R@50	mR@20	mR@50
Final	<b>21.8</b>	<b>28.0</b>	<b>4.6</b>	<b>7.4</b>
Top 3 inst labels	21.3	27.8	4.0	6.2
Top 1 inst label	21.8	27.6	4.4	6.9
Bbox nms 0.7	21.2	27.7	4.5	6.8
Bbox nms 0.3	21.6	27.4	4.5	7.2

Table 5. Ablation studies on Visual Genome. Top one results are shown in **bold**. In PredCLS, “no rel-hierarchy” means using a flat relationship classification instead of the Bayes prediction head. “no ins-hierarchy” means ignoring instance super-categories in the predictor. “no depth map” means ignoring image depth maps. “union bbox” means using a union bounding box of the subject-object pairs, not the direction-aware scheme. “add tf-enc” refers to adding the optional transformer encoder networks on top of the local prediction scheme, where  $s$  is the sparsity of the relationships seen by the encoder. In the SGDET, the final baseline mode uses the top two highest-rated object categories per predicted bounding box, with a per-class NMS of 0.5. The last several rows show the results obtained by varying these two parameters. Overall, the results show that instance and relationship hierarchies significantly improve relationship predictions. Meanwhile, the optional transformer encoder improves mR@ $k$  but sacrifices R@ $k$  marginally.

## 5. Concluding remarks

We present a simple but powerful scene graph generation algorithm that exploits a hierarchical categorical structure imposed on the relationship and object labels. The resulting system has a Bayesian structure with separate heads that predict the likelihood of a relationship between a pair of objects, the super-category of that relationship if it exists, and the specific relationship within each super-category. This representation effectively factorizes the final probability distribution over the relationship categories.

Our results show that the hierarchical organization significantly outperforms a baseline that predicts a flat softmax over all relationship types. Our scheme performs competitively with state-of-the-art algorithms, especially in predicate classification and zero-shot learning. We hypothesize that this structure allows related labels to more effectively share the information common to each super-category.

We note that the proposed hierarchical approach could also be applied to other classification tasks and we plan to explore this possibility in future work.

## References

- [1] Nicolas Carion, Francisco Massa, Gabriel Synnaeve, Nicolas Usunier, Alexander Kirillov, and Sergey Zagoruyko. End-to-end object detection with transformers. In *European conference on computer vision*, pages 213–229. Springer, 2020. [1](#), [2](#), [3](#), [8](#)
- [2] Liang-Chieh Chen, George Papandreou, Iasonas Kokkinos, Kevin Murphy, and Alan L Yuille. Deeplab: Semantic image segmentation with deep convolutional nets, atrous convolution, and fully connected crfs. *IEEE transactions on pattern analysis and machine intelligence*, 40(4):834–848, 2017. [1](#)
- [3] Tianshui Chen, Weihao Yu, Riquan Chen, and Liang Lin. Knowledge-embedded routing network for scene graph generation. In *Proceedings of the IEEE/CVF Conference on Computer Vision and Pattern Recognition*, pages 6163–6171, 2019. [2](#)
- [4] Kyunghyun Cho, Bart Van Merriënboer, Dzmitry Bahdanau, and Yoshua Bengio. On the properties of neural machine translation: Encoder-decoder approaches. *arXiv preprint arXiv:1409.1259*, 2014. [2](#)
- [5] Yuren Cong, Michael Ying Yang, and Bodo Rosenhahn. Reltr: Relation transformer for scene graph generation. *arXiv preprint arXiv:2201.11460*, 2022. [2](#), [7](#)
- [6] Naina Dhingra, Florian Ritter, and Andreas Kunz. Bgtnet: Bidirectional gru transformer network for scene graph generation. In *Proceedings of the IEEE/CVF Conference on Computer Vision and Pattern Recognition*, pages 2150–2159, 2021. [2](#), [3](#), [7](#), [8](#)
- [7] Alexey Dosovitskiy, Lucas Beyer, Alexander Kolesnikov, Dirk Weissenborn, Xiaohua Zhai, Thomas Unterthiner, Mostafa Dehghani, Matthias Minderer, Georg Heigold, Sylvain Gelly, et al. An image is worth 16x16 words: Transformers for image recognition at scale. *arXiv preprint arXiv:2010.11929*, 2020. [4](#)
- [8] Kaiming He, Georgia Gkioxari, Piotr Dollár, and Ross Girshick. Mask r-cnn. In *Proceedings of the IEEE international conference on computer vision*, pages 2961–2969, 2017. [1](#)
- [9] Kaiming He, Xiangyu Zhang, Shaoqing Ren, and Jian Sun. Deep residual learning for image recognition. In *Proceedings of the IEEE conference on computer vision and pattern recognition*, pages 770–778, 2016. [3](#)
- [10] Sepp Hochreiter and Jürgen Schmidhuber. Long short-term memory. *Neural computation*, 9(8):1735–1780, 1997. [2](#)
- [11] Justin Johnson, Ranjay Krishna, Michael Stark, Li-Jia Li, David Shamma, Michael Bernstein, and Li Fei-Fei. Image retrieval using scene graphs. In *Proceedings of the IEEE conference on computer vision and pattern recognition*, pages 3668–3678, 2015. [1](#), [2](#)
- [12] Mahmoud Khademi and Oliver Schulte. Deep generative probabilistic graph neural networks for scene graph generation. In *Proceedings of the AAAI Conference on Artificial Intelligence*, volume 34, pages 11237–11245, 2020. [2](#)
- [13] Thomas N Kipf and Max Welling. Semi-supervised classification with graph convolutional networks. *arXiv preprint arXiv:1609.02907*, 2016. [2](#)
- [14] Rajat Koner, Suprosanna Shit, and Volker Tresp. Relation transformer network. *arXiv preprint arXiv:2004.06193*, 2020. [2](#)
- [15] Ranjay Krishna, Yuke Zhu, Oliver Groth, Justin Johnson, Kenji Hata, Joshua Kravitz, Stephanie Chen, Yannis Kalantidis, Li-Jia Li, David A Shamma, et al. Visual genome: Connecting language and vision using crowdsourced dense image annotations. *International journal of computer vision*, 123(1):32–73, 2017. [2](#), [5](#)
- [16] Alina Kuznetsova, Hassan Rom, Neil Alldrin, Jasper Uijlings, Ivan Krasin, Jordi Pont-Tuset, Shahab Kamali, Stefan Popov, Matteo Mallocci, Alexander Kolesnikov, et al. The open images dataset v4: Unified image classification, object detection, and visual relationship detection at scale. *International Journal of Computer Vision*, 128(7):1956–1981, 2020. [5](#)
- [17] Rongjie Li, Songyang Zhang, and Xuming He. Sgr: End-to-end scene graph generation with transformer. In *Proceedings of the IEEE/CVF Conference on Computer Vision and Pattern Recognition*, pages 19486–19496, 2022. [5](#), [6](#)
- [18] Xin Lin, Changxing Ding, Jinquan Zeng, and Dacheng Tao. Gps-net: Graph property sensing network for scene graph generation. In *Proceedings of the IEEE/CVF Conference on Computer Vision and Pattern Recognition*, pages 3746–3753, 2020. [2](#), [3](#), [7](#), [8](#)
- [19] Wei Liu, Dragomir Anguelov, Dumitru Erhan, Christian Szegedy, Scott Reed, Cheng-Yang Fu, and Alexander C Berg. Ssd: Single shot multibox detector. In *European conference on computer vision*, pages 21–37. Springer, 2016. [1](#)
- [20] Jonathan Long, Evan Shelhamer, and Trevor Darrell. Fully convolutional networks for semantic segmentation. In *Proceedings of the IEEE conference on computer vision and pattern recognition*, pages 3431–3440, 2015. [1](#)
- [21] Ilya Loshchilov and Frank Hutter. Decoupled weight decay regularization. *arXiv preprint arXiv:1711.05101*, 2017. [7](#)
- [22] Cewu Lu, Ranjay Krishna, Michael Bernstein, and Li Fei-Fei. Visual relationship detection with language priors. In *European conference on computer vision*, pages 852–869. Springer, 2016. [2](#), [5](#)
- [23] Roozbeh Mottaghi, Xianjie Chen, Xiaobai Liu, Nam-Gyu Cho, Seong-Whan Lee, Sanja Fidler, Raquel Urtasun, and Alan Yuille. The role of context for object detection and semantic segmentation in the wild. In *Proceedings of the IEEE conference on computer vision and pattern recognition*, pages 891–898, 2014. [1](#)
- [24] Alejandro Newell and Jia Deng. Pixels to graphs by associative embedding. *Advances in neural information processing systems*, 30, 2017. [5](#)
- [25] Aude Oliva and Antonio Torralba. The role of context in object recognition. *Trends in cognitive sciences*, 11(12):520–527, 2007. [1](#)
- [26] René Ranftl, Katrin Lasinger, David Hafner, Konrad Schindler, and Vladlen Koltun. Towards robust monocular depth estimation: Mixing datasets for zero-shot cross-dataset transfer. *IEEE transactions on pattern analysis and machine intelligence*, 2020. [3](#)

[27] Joseph Redmon, Santosh Divvala, Ross Girshick, and Ali Farhadi. You only look once: Unified, real-time object detection. In *Proceedings of the IEEE conference on computer vision and pattern recognition*, pages 779–788, 2016. 1

[28] Guanghui Ren, Lejian Ren, Yue Liao, Si Liu, Bo Li, Jizhong Han, and Shuicheng Yan. Scene graph generation with hierarchical context. *IEEE Transactions on Neural Networks and Learning Systems*, 32(2):909–915, 2020. 2, 7

[29] Shaoqing Ren, Kaiming He, Ross Girshick, and Jian Sun. Faster r-cnn: Towards real-time object detection with region proposal networks. *Advances in neural information processing systems*, 28, 2015. 1, 5

[30] Olaf Ronneberger, Philipp Fischer, and Thomas Brox. U-net: Convolutional networks for biomedical image segmentation. In *International Conference on Medical image computing and computer-assisted intervention*, pages 234–241. Springer, 2015. 1

[31] Franco Scarselli, Marco Gori, Ah Chung Tsoi, Markus Hagenbuchner, and Gabriele Monfardini. The graph neural network model. *IEEE transactions on neural networks*, 20(1):61–80, 2008. 2

[32] Karen Simonyan and Andrew Zisserman. Very deep convolutional networks for large-scale image recognition. *arXiv preprint arXiv:1409.1556*, 2014. 3

[33] Mohammed Suhail, Abhay Mittal, Behjat Siddique, Chris Broaddus, Jayan Eledath, Gerard Medioni, and Leonid Sigal. Energy-based learning for scene graph generation. In *Proceedings of the IEEE/CVF conference on computer vision and pattern recognition*, pages 13936–13945, 2021. 2, 7

[34] Kaihua Tang, Yulei Niu, Jianqiang Huang, Jiaxin Shi, and Hanwang Zhang. Unbiased scene graph generation from biased training. In *Proceedings of the IEEE/CVF conference on computer vision and pattern recognition*, pages 3716–3725, 2020. 5

[35] Kaihua Tang, Hanwang Zhang, Baoyuan Wu, Wenhan Luo, and Wei Liu. Learning to compose dynamic tree structures for visual contexts. In *Proceedings of the IEEE/CVF conference on computer vision and pattern recognition*, pages 6619–6628, 2019. 5

[36] Ashish Vaswani, Noam Shazeer, Niki Parmar, Jakob Uszkoreit, Llion Jones, Aidan N Gomez, Łukasz Kaiser, and Illia Polosukhin. Attention is all you need. *Advances in neural information processing systems*, 30, 2017. 3, 4, 5, 7

[37] Danfei Xu, Yuke Zhu, Christopher B Choy, and Li Fei-Fei. Scene graph generation by iterative message passing. In *Proceedings of the IEEE conference on computer vision and pattern recognition*, pages 5410–5419, 2017. 2, 3, 5, 7

[38] Minghao Xu, Meng Qu, Bingbing Ni, and Jian Tang. Joint modeling of visual objects and relations for scene graph generation. *Advances in Neural Information Processing Systems*, 34:7689–7702, 2021. 2

[39] Jianwei Yang, Jiasen Lu, Stefan Lee, Dhruv Batra, and Devi Parikh. Graph r-cnn for scene graph generation. In *Proceedings of the European conference on computer vision (ECCV)*, pages 670–685, 2018. 2, 3, 7

[40] Jiaxuan You, Rex Ying, Xiang Ren, William Hamilton, and Jure Leskovec. Graphrnn: Generating realistic graphs with deep auto-regressive models. In *International conference on machine learning*, pages 5708–5717. PMLR, 2018. 3

[41] Rowan Zellers, Mark Yatskar, Sam Thomson, and Yejin Choi. Neural motifs: Scene graph parsing with global context. In *Proceedings of the IEEE conference on computer vision and pattern recognition*, pages 5831–5840, 2018. 1, 2, 3, 5, 6, 7

[42] Ji Zhang, Kevin J Shih, Ahmed Elgammal, Andrew Tao, and Bryan Catanzaro. Graphical contrastive losses for scene graph parsing. In *Proceedings of the IEEE/CVF Conference on Computer Vision and Pattern Recognition*, pages 11535–11543, 2019. 5, 8